Quantum simulation of spin models on an arbitrary lattice with trapped ions

New Journal of Physics

Quantum simulation of spin models on an arbitrary lattice with trapped ions

S Korenblit[1,5]**, D Kafri**[1]**, W C Campbell**[1]**, R Islam**[1]**, E E Edwards**[1]**, Z-X Gong**[2]**, G-D Lin**[2]**, L-M Duan**[2]**, J Kim**[3]**, K Kim**[4] **and C Monroe**[1]

[1] Joint Quantum Institute, University of Maryland Department of Physics and National Institute of Standards and Technology, College Park, MD 20742, USA
[2] Department of Physics and MCTP, University of Michigan, Ann Arbor, MI 48109, USA
[3] Fitzpatrick Institute for Photonics, Department of Electrical and Computer Engineering, Duke University, Durham, NC 27708, USA
[4] Center for Quantum Information, Tsinghua University, Beijing 100084, People's Republic of China
E-mail: simchak@umd.edu

Abstract. A collection of trapped atomic ions represents one of the most attractive platforms for the quantum simulation of interacting spin networks and quantum magnetism. Spin-dependent optical dipole forces applied to an ion crystal create long-range effective spin–spin interactions and allow the simulation of spin Hamiltonians that possess nontrivial phases and dynamics. Here we show how the appropriate design of laser fields can provide for arbitrary multidimensional spin–spin interaction graphs even for the case of a linear spatial array of ions. This scheme uses currently available trap technology and is scalable to levels where the classical methods of simulation are intractable.

[5] Author to whom any correspondence should be addressed.

Quantum systems are notoriously difficult to model efficiently using classical computers, owing to the exponential complexity in describing a general quantum state as the system grows in size. In the 1980s, Richard Feynman proposed to circumvent this problem by employing a control quantum system with tailored interactions and logic gates between quantum bits (qubits) in order to simulate the quantum system under investigation [1, 2].

Quantum spin models such as the Ising model have become a proving ground for Feynman's proposal, with systems of qubits behaving as effective spins and interactions engineered with external electromagnetic fields. The quantum Ising model is the simplest spin Hamiltonian that exhibits nontrivial aspects of quantum magnetism such as spin frustration, phase transitions [3] and poorly understood spin glass and spin liquid phases [4, 5]. Indeed, solving for the ground state configuration of spins subject to a general fully connected Ising interaction is known to be an NP-complete problem [6]. Here we show how a fully connected Ising or more general Heisenberg spin model with arbitrary couplings across the spin network can be generated in a scalable system of trapped atomic ions, even for a one-dimensional (1D) chain in space. This may allow quantum simulations with hundreds of spins, where the physics cannot generally be predicted otherwise.

Isolated atoms are an ideal control quantum system for quantum simulations, as they exhibit very long coherence times, can be measured with high efficiency and can obviously be replicated with nearly identical characteristics. There has been great progress in the use of atoms trapped in optical lattices for the studies of transport phenomena such as those described by the Hubbard models [7] and the fractional quantum Hall effect [8]. Following original proposals to exploit atomic ions for the simulation of spin models [9–11], there has been steady progress in simulating Ising models with an effective transverse magnetic field, showing the behavior of quantum phase transitions in the limit of less than ten spins [12–18]. Recently, the Ising model with an axial field was demonstrated in neutral atoms in optical lattices with nearest-neighbor couplings [19]. All these studies involve global spin-dependent optical dipole forces to generate trivial forms of the spin couplings, such as a uniform ferromagnet. Below we show how to tailor optical forces to generate arbitrary fully connected networks of N spins that uniquely specify each of the $N(N-1)/2$ pairwise interactions. The scheme is independent of the spatial geometry of the ion crystal and is compatible with 1D arrays of trapped ions used in current experiments.

We start with the arbitrary fully connected Ising Hamiltonian on N spins,

$$H = \sum_{i<j} J_{i,j} \sigma_x^{(i)} \sigma_x^{(j)}, \tag{1}$$

where the matrix $J_{i,j}$ is the strength of the spin–spin coupling between atoms i and j. The Pauli spin operator $\sigma_x^{(i)}$ refers to the effective spin-1/2 system within each atom, here represented, for example, by a pair of hyperfine ground states separated by frequency ω_s [20].

The spins are coherently manipulated through a pair of counter-propagating laser beams that drive stimulated Raman transitions between the spin states while also coupling off-resonantly to the collective motion of the atomic chain [21, 22]. The atoms are arranged in a linear array, as is typical in a linear radiofrequency ion trap, although this scheme can also apply to other spatial geometries [11, 23, 24]. When the difference frequency between the Raman fields is bichromatic, with two spectral components tuned symmetrically at $\omega_s \pm \mu$ with
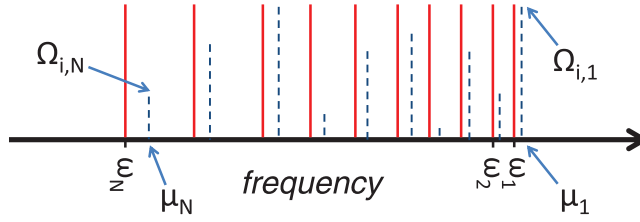
Figure 1. Spectrum of transverse mode frequencies ω_m for $N = 10$ ions in an anisotropic harmonic linear trap (solid lines), with the highest mode frequency ω_1 corresponding to the center-of-mass (COM) motion. Raman beatnote detunings μ_m from the qubit frequency ω_s are denoted by the $N = 10$ dashed lines, with each spectral feature near a given motional sideband. The height of the dashed lines represents the intensity of each beatnote for ion i. In general, each ion will be illuminated with a different set of intensities.

$\mu \ll \omega_s$, the effective spin–spin interaction of equation (1) emerges, mediated by the Coulomb-coupled motion of the atomic ions crystal [25, 26]. The axis of the spin–spin interaction on the Bloch sphere can be controlled by the relative optical phase of the two Raman fields [27, 28]. We assume that the Raman lasers have wave vector difference δk along the principal X-axis of transverse motion of the ion crystal [29] so that each X-transverse normal mode m with frequency ω_m contributes to each spin–spin coupling [13],

$$J_{i,j} = \Omega_i \Omega_j \sum_{m=1}^{N} \frac{\eta_{i,m} \eta_{j,m} \omega_m}{\mu^2 - \omega_m^2}. \tag{2}$$

Here, the Lamb–Dicke parameter $\eta_{i,m} = b_{i,m} \delta k \sqrt{\hbar/(2M\omega_m)}$ sets the scale for the coupling between spin i and mode m, $b_{i,m}$ is the normal mode transformation matrix, M is the mass of a single atom, and the single spin Rabi frequency Ω_i is proportional to the optical intensity at atom i. The above expression is valid when the transverse modes are all laser-cooled to the Lamb–Dicke limit [21, 30], which is routine in typical linear traps [13]. We also assume that the symmetric detuning μ is set sufficiently far from all motional sidebands ($|\omega_m - \mu| \gg \eta_{i,m}\Omega_i$), so that the phonon states can be adiabatically eliminated, leaving the pure spin–spin coupling above [13, 25, 26].

The above expression has $N + 1$ control parameters in the set of Rabi frequencies $\{\Omega_i\}$ and the global beatnote detuning μ. In order to generate an arbitrary Ising coupling matrix $J_{i,j}$ however, it is necessary to have at least $N(N-1)/2$ independent controls [31]. Additional control parameters can be introduced by adding multiple spectral beatnote detunings to the Raman beams, one near each motional mode (see figure 1), with a unique pattern of spectral components on each ion. There are several ways to achieve this, all involving some form of individual ion addressing. For simplicity, we retain the same set of N Raman beatnote detunings $\{\mu_m\}$ on each ion and allow the spectral amplitude pattern to vary between ions, all characterized by the $N \times N$ Rabi frequency matrix $\Omega_{i,n}$ of spectral component n at ion i. Note that the relative signs of the Rabi frequency matrix elements can be controlled by adjusting the phase of each spectral component. This individual spectral amplitude addressing provides N^2 control

parameters, and the general Ising coupling matrix becomes

$$J_{i,j} = \sum_{n=1}^{N} \Omega_{i,n}\Omega_{j,n} \sum_{m=1}^{N} \frac{\eta_{i,m}\eta_{j,m}\omega_m}{\mu_n^2 - \omega_m^2} \tag{3}$$
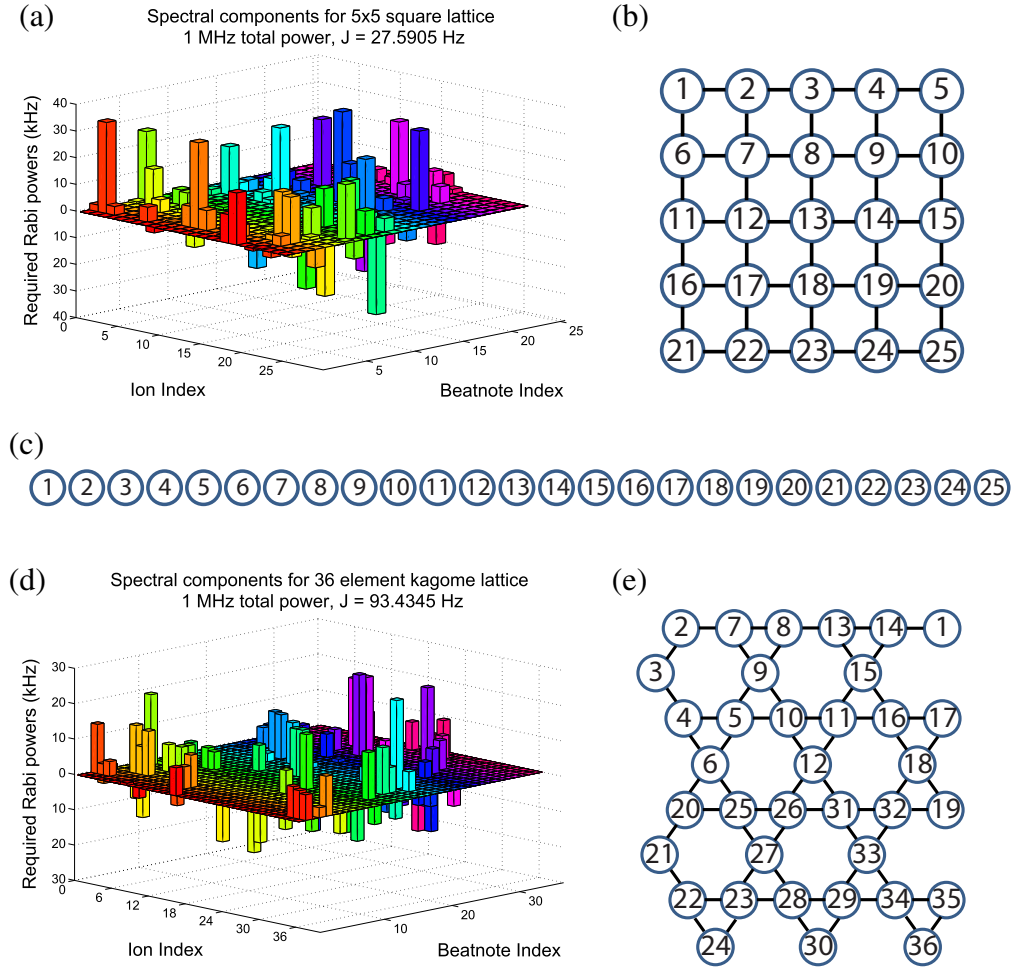
$$\equiv \sum_{n=1}^{N} \Omega_{i,n}\Omega_{j,n}F_{i,j,n}, \tag{4}$$

where $F_{i,j,n}$ characterizes the response of Ising coupling $J_{i,j}$ to spectral component n. An exact derivation of the effective Hamiltonian given a spectrum of spin-dependent forces gives rise to new off-resonant cross terms, which can be shown to be negligible in the rotating wave approximation, as long as the bandwidth is fixed and the transverse COM mode is set to a frequency smaller than twice the transverse zigzag mode frequency. Thus the sums and differences of beatnotes do not directly encroach on any sideband features in the motional spectrum of the crystal [29].

We tune each beatnote frequency near a unique normal mode so that $F_{i,j,n}$ has independent contributions for each n. Given a desired Ising coupling matrix $J_{i,j}$, we use standard constrained nonlinear optimization to find the corresponding Rabi frequency matrix $\Omega_{i,n}$, while minimizing the total beam intensity. The deviation between the desired and the attained coupling was less than typical round-off errors.

We now present two example solutions for $\Omega_{i,n}$ that produce interesting interaction graph topologies. First we calculate a Rabi frequency matrix that results in a 2D square lattice of nearest-neighbor antiferromagnetic couplings with $N = 25$ ions (a 5×5 grid with periodic boundary conditions), shown in figures 2(a) and (b). Next, we produce a 2D Kagome lattice of antiferromagnetic interactions, a geometry that can support high levels of geometrical frustration [32], shown in figures 2(d) and (e). In both cases, we assume the COM mode to be $\omega_1/2\pi = 5\,\text{MHz}$, and a fixed total optical intensity corresponding to $\sum_{i,n} |\Omega_{i,n}| = 1\,\text{MHz}$. The beatnote frequencies μ_m are each tuned blue of the mode m sideband by a fraction f_s of the spacing $\omega_1 - \omega_2$ between the most closely spaced modes (the COM and 'tilt' modes, see figure 1), which itself scales as $\log N/N^2$. In these examples, the sparse nearest-neighbor nature of the interaction graphs requires that most of the Ising interactions vanish, indicating a high level of coherent control over all of the Ising couplings.

In order to generate a unique spectrum of Raman beams for each of N ions, some type of individual addressing is necessary. For simplicity, we assume that one of the two Raman beams is uniform and monochromatic, and the high-frequency beatnote near the qubit frequency ω_s or other global offset frequencies can be set by tuning this monochromatic beam. We focus on providing the requisite frequencies of the second beam, spread over a range given by the bandwidth of the transverse motional mode frequencies of the ion chain, typically in the range 1–5 MHz. We suggest three possible methods for providing spatial dependent frequency modulation to one of the Raman beams. The first method (figure 3) splits a single beam with a linear chain of N individual optical modulators (e.g. acousto-optic or electro-optic devices), driven by N independent arbitrary waveform generators. The second method splits a single monochromatic beam into an $N \times N$ square grid and directs them onto a 2D array of N^2 micromirrors [33] that are each individually phase modulated at a single frequency (and phase) [34] and are finally focused on the ion chain. The third method again splits the beam into an $N \times N$ grid of beams, this time with the vertical direction split by a single acousto-optic

(a)

Spectral components for 5x5 square lattice
1 MHz total power, J = 27.5905 Hz

(b)

(c)

(d)

Spectral components for 36 element kagome lattice
1 MHz total power, J = 93.4345 Hz

(e)

Figure 2. (a) Calculated Rabi frequency matrix $\Omega_{i,n}$ to generate two-dimensional (2D) square lattice shown in (b), using the linear chain of $N = 25$ ions shown in (c). The ion index refers to the order in the linear chain. The attained $J_{i,j}$ nearest-neighbor is 27.6 Hz for $f_s = 0.1$. (d) Calculated Rabi frequency matrix $\Omega_{i,n}$ to generate 2D Kagome lattice shown in (e) using a linear chain of $N = 36$ ions. The attained $J_{i,j}$ nearest-neighbor is 93.4 Hz for $f_s = 0.03$. In both cases the total optical intensity corresponds to a Rabi frequency of 1 MHz if focused on a single ion, the nearest-neighbor couplings are antiferromagnetic and we impose periodic boundary conditions.

modulator, correlating the beam position to frequency. This beam is then directed into a spatial light modulator that acts to mask (or phase shift) each of the $N \times N$ beams independently, and again focused onto the ion chain. In these implementations, it may be desirable to work with a uniformly spaced array of ions in the linear trap, so that the modulating elements are also uniformly spaced. This can be accomplished by using a quartic or higher order linear trap [35, 36].

As the number of spins N grows, the optical modulation scheme becomes more complex, with either N or N^2 elements required. However, our schemes restrict most of the resources'
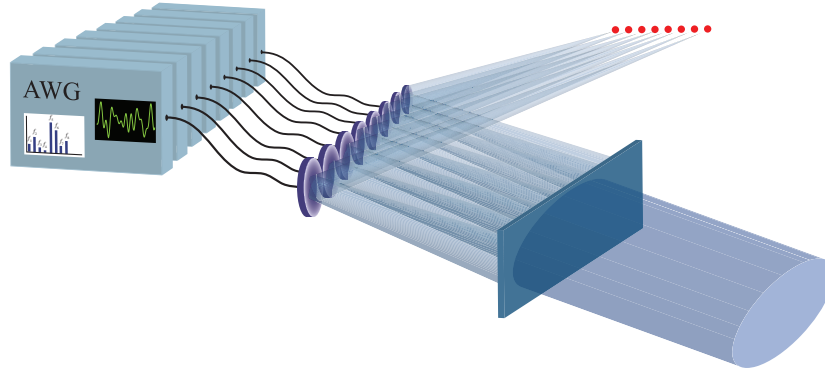
Figure 3. Schematic diagram of individual spectral addressing of a linear chain of N ions. A laser beam is split into a linear array of spots that each traverse N independent acousto- or electro-optical modulators, driven by N independent arbitrary waveform generators (AWG). Alternatively, as discussed in the text, the beam can be broken into an array of N^2 beams that strike an $N \times N$ array of micromirrors each independently modulated, or a spatial light modulator.

overhead to the design and fabrication of the micro-mirrors or phase modulator. As the ions are equally spaced, the modulator can simply be imaged onto the ion chain without changing imaging optics.

We now estimate how the Ising couplings are expected to scale with the number of spins along with errors due to experimental fluctuations, phonon creation and spontaneous emission scattering, assuming a fixed transverse mode bandwidth. The probability of phonon creation scales as $p_{ph} = \sum_{i,m} \left(\frac{\eta_{i,m} \Omega_{i,m}}{\omega_m - \mu_m} \right)^2$. The off-resonant optical dipole forces are accompanied by a finite rate of spontaneous emission scattering, given by $\Gamma = \epsilon \sum_{i,m} |\Omega_{i,m}|$, where $\epsilon \ll 1$ is the ratio of the excited state linewidth to Raman detuning. The scaling of these potential errors depends upon the particular graph, so we consider two extremes. A uniform fully connected interaction graph can be trivially generated with a single spectral component tuned close to the COM mode with a detuning $|\omega_1 - \mu|/\omega_1 \ll \log N/N^2$. For a fixed level of phonon error, the total optical intensity should be reduced as $\log N/N$, taking into account the intensity reduction per ion as the beam is expanded to accommodate the linearly expanding chain in space. In this case the uniform Ising coupling is expected to scale as $N|J_{i,j}| \propto \log N/N^2$, and the spontaneous emission rate per spin actually decreases with N. For a sparse interaction graph, such as a 1D (nearest-neighbor) Ising model, all modes are involved, and this time for a fixed phonon error the total optical intensity can remain fixed, since the typical mode splitting falls only as $1/N$, while spontaneous emission per ion is fixed. The calculation in figure 4 shows that the resulting nearest-neighbor interaction scales as $J_{i,i+1} \propto 1/N$. In the case of a fully connected or local Ising model, we thus expect to be able to support significant Ising interaction strengths with up to a few hundreds of spins.

For a general Ising graph, from equation (4) we find that each pairwise interaction $J_{i,j}$ depends upon a balance of N terms, and errors will accumulate with N from fluctuations of relative optical intensities of the various spectral components of the beam (which should be stable if the spectral components are generated with high-quality radiofrequency sources and modulators as shown in figure 3) or their detunings from the motional sidebands. The most
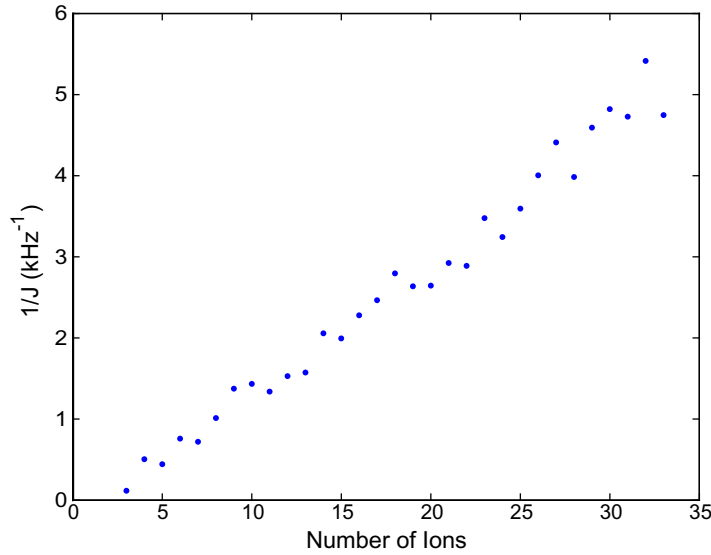
Figure 4. Scaling of the nearest-neighbor coupling for the case of the production of a 1D Ising chain for $N = 3$ up to $N = 33$ ions. The total optical intensity is fixed at $\sum_{i,n} |\Omega_{i,n}| = 1$ MHz, and each spectral component is detuned from its motional sideband by a fraction $f_s = 0.03$ of the smallest mode splitting, with a COM frequency of $\omega_1/2\pi = 5$ MHz. We find that the resulting Ising coupling scales roughly as $1/N$.

important source will likely be fluctuations in the motional trap frequencies, where we expect the fractional error in the Ising coupling to grow as $\sqrt{N}(\delta\omega_m/\omega_m)$, so that a typical fractional fluctuation in the motional trapping frequencies of $\sim 10^{-3}$ might be expected to cause Ising coupling errors at the level of about 1% for $N \sim 100$ ions.

The final limitation on simulation time is effective spin coherence. Assuming that the qubits experience Markovian noise, the coherence time of the ensemble will go as $1/N$, so that a qubit coherence time of ~ 10 s (as is typical of hyperfine qubits) will allow for a simulation time of the order of ~ 100 ms for ~ 100 ions.

The scheme presented here can also be applied to more general Heisenberg spin models involving other noncommuting spin–spin interactions, such as the *XY* model or the 2D hexagonal Kitaev model relevant to topological quantum degrees of freedom [37]. Here, additional Raman beams that couple to the other axes of motion can be exploited [9]. This scheme may also be used to study phase transitions in a quantum transverse magnetic field [38]. Although this discussion concentrated on a linear array of ions in space, these ideas apply in general to any stable ion crystal where the motional sidebands are resolved and prepared in the Lamb–Dicke limit, and should be useful for higher-dimensional trap geometries such as trap arrays [23, 24] or Penning traps [11, 39].

Acknowledgments

References

[1] Feynman R 1982 *Int. J. Theor. Phys.* **21** 467
[2] Lloyd S 1996 *Science* **273** 1073
[3] Sachdev S 2011 *Quantum Phase Transitions* (Cambridge: Cambridge University Press)
[4] Binder K and Young A P 1986 *Rev. Mod. Phys.* **58** 801
[5] Balents L 2010 *Nature* **464** 199
[6] Cipra B A 2000 *SIAM News* **33** 6
[7] Bloch I, Dalibard J and Zwerger W 2008 *Rev. Mod. Phys.* **80** 885
[8] Lin Y-J, Compton R L, Jimenez-Garcia K, Phillips W D, Porto J V and Spielman I B 2011 *Nature Phys.* **7** 531
[9] Porras D and Cirac J I 2004 *Phys. Rev. Lett.* **92** 207901
[10] Deng X L, Porras D and Cirac J I 2005 *Phys. Rev.* A **72** 063407
[11] Taylor J M and Calarco T 2008 *Phys. Rev.* A **78** 062331
[12] Friedenauer A, Schmitz H, Glueckert J T, Porras D and Schaetz T 2008 *Nature Phys.* **4** 757
[13] Kim K, Chang M-S, Islam R, Korenblit S, Duan L-M and Monroe C 2009 *Phys. Rev. Lett.* **103** 120502
[14] Kim K, Chang M-S, Korenblit S, Islam R, Edwards E E, Freericks J, Lin G, Duan L-M and Monroe C 2010 *Nature* **465** 590
[15] Edwards E E, Korenblit S, Kim K, Islam R, Chang M-S, Freericks J K, Lin G-D, Duan L-M and Monroe C 2010 *Phys. Rev.* B **82** 060412
[16] Barreiro J T, Müller M, Schindler P, Nigg D, Monz T, Chwalla M, Hennrich M, Roos C F, Zoller P and Blatt R 2010 *Nature* **470** 486
[17] Islam R *et al* 2011 *Nature Commun.* **2**
[18] Lanyon B P *et al* 2011 *Science* **334** 57–61
[19] Simon J, Bakr W S, Ma R, Tai M E, Preiss P M and Greiner M 2011 *Nature* **472** 307
[20] Olmschenk S, Younge K C, Moehring D L, Matsukevich D N, Maunz P and Monroe C 2007 *Phys. Rev.* A **76** 052314
[21] Wineland D J, Monroe C, Itano W M, Leibfried D, King B E and Meekhof D M 1998 *J. Res. Natl Inst. Stand. Technol.* **103** 259
[22] Wineland D and Blatt R 2008 *Nature* **453** 1008
[23] Clark R J, Linb T, Brown K R and Chuang I L 2009 *J. Appl. Phys.* **105** 013114
[24] Schmied R, Wesenberg J H and Leibfried D 2009 *Phys. Rev. Lett.* **102** 233002
[25] Sørensen A and Mølmer K 1999 *Phys. Rev. Lett.* **82** 1971
[26] Sørensen A and Mølmer K 2000 *Phys. Rev.* A **62** 022311
[27] Haljan P C, Brickman K-A, Deslauriers L, Lee P J and Monroe C 2005 *Phys. Rev. Lett.* **94** 153602
[28] Lee P J, Brickman K-A, Deslauriers L, Haljan P C, Duan L-M and Monroe C 2005 *J. Opt. B: Quantum Semiclass. Opt.* **7** S371
[29] Zhu S-L, Monroe C and Duan L-M 2006 *Phys. Rev. Lett.* **97** 050505
[30] Leibfried D, Blatt R, Monroe C and Wineland D 2003 *Rev. Mod. Phys.* **75** 281
[31] García-Ripoll J J, Zoller P and Cirac J I 2005 *Phys. Rev.* A **71** 062309
[32] Moessner R and Ramirez A P 2006 *Phys. Today* **59** 24
[33] Knoernschild C, Zhang X L, Isenhower L, Gill A T, Lu F P, Saffman M and Kim J 2010 *Appl. Phys. Lett.* **97** 134101
[34] Knoernschild C, Kim T, Maunz P, Crain S and Kim J 2012 *Opt. Express* **20** 3261–7
[35] Lin G-D, Zhu S-L, Islam R, Kim K, Chang M-S, Korenblit S, Monroe C and Duan L-M 2009 *Eur. Phys. Lett.* **86** 60004

IOP Institute of Physics ⊕ DEUTSCHE PHYSIKALISCHE GESELLSCHAFT

[36] Shaikh F, Ozakin A, Amini J M, Hayden H, Pai C-S, Volin C, Denison D R, Faircloth D, Harter A W and Slusher R E 2011 arXiv:1105.4909
[37] Kitaev A 2006 *Ann. Phys.* **321** 2
[38] Rams M M, Zwolak M and Damski B 2012 arXiv:1201.1932
[39] Biercuk M J, Uys H, Vandevender A P, Shiga N, Itano W M and Bollinger J J 2011 *Quantum Inform. Comput.* **9** 920